Self-Assembled Complexes of Poly(4-vinylphenol) and Poly(ε-caprolactone)-*block*-poly(2-vinylpyridine) via Competitive Hydrogen Bonding

Nishar Hameed, Jing Liu, and Qipeng Guo*

Centre for Material and Fibre Innovation, Deakin University, Geelong, Victoria 3217, Australia

Received March 29, 2008; Revised Manuscript Received August 7, 2008

ABSTRACT: Nanostructured complexes were prepared from poly(ε-caprolactone)-*block*-poly(2-vinylpyridine) (PCL-*b*-P2VP) and poly(4-vinylphenol) (PVPh) in tetrahydrofuran (THF). The phase behavior, specific interactions, and morphology were investigated using differential scanning calorimetry (DSC), Fourier transform infrared (FTIR) spectroscopy, optical microscopy, atomic force microscopy (AFM), transmission electron microscopy (TEM), and small-angle X-ray scattering (SAXS). In this A-*b*-B/C type block copolymer/homopolymer system, both blocks of the PCL-*b*-P2VP block copolymer have favorable intermolecular interaction toward PVPh via hydrogen bonding, but the interaction between P2VP block and PVPh is significantly stronger than that between PCL block and PVPh. It was found that the disparity in competitive intermolecular interactions, specifically PVPh and P2VP block interact strongly whereas PVPh and PCL block interact weakly, leads to the formation of a variety of nanostructures depending on PVPh concentration. Spherical micelles of 30−40 nm in diameter were obtained in the complex with 10 wt % PVPh, followed by wormlike micelles with size in the order of 40−50 nm in the complexes with 30−60 wt % PVPh. At low PVPh concentrations, PCL interacts weakly with PVPh, whereas in the complexes containing more than 20 wt % PVPh, the PCL block began to interact considerably with PVPh, leading to the formation of composition-dependent nanostructures. The complex becomes homogeneous with PVPh content beyond 60 wt %, since a sufficient amount of PVPh is available to form hydrogen bonds with both PCL and P2VP. Finally, a model was proposed to explain the self-assembly and microphase morphology of these complexes based on the experimental results obtained. The competitive hydrogen-bonding interactions cause the self-assembly and formation of different microphase morphologies.

Introduction

Polymer mixtures containing block copolymers that exhibit fascinating self-assembly behavior have attracted much attention for the use as functional nanostructures.[1−9] The size and shape of these nanostructures can be controlled by changing the parameters such as molecular weights, chemical structure, and composition of the block copolymer in the mixture. Moreover, a range of ordered structures can be created in block copolymer mixtures, depending on the number of blocks, their volume fraction, chain flexibility, and the extent of repulsion between the chemically connected blocks. In block copolymer/homopolymer mixtures, attraction or repulsion between similar or different blocks leads to the self-assembly into spherical, lamellar, cylindrical or wormlike, and other nanostructures. In a diblock copolymer/homopolymer system,[10−13] ordered structures can be established in different ways, including (1) the smectic order resulting from the covalently bonded mesogenic side groups and (2) the ordered microphases formation used by the secondary interactions such as hydrogen bonding, coordination bonding, ionic interactions, etc. Among these, the introduction of hydrogen-bonding interactions into the block polymer blend systems provides a new mechanism of self-assembling, which may lead to production of highly functional polymeric materials.

However, most of the studies reported so far involve the blends of A-*b*-B/C diblock copolymer/homopolymer where the homopolymer C is immiscible with B but interacts favorably with A. Our previous work studied the selective hydrogen bonding and hierarchical nanostructures in poly(hydroxy ether of bisphenol A) (phenoxy)/poly(ε-caprolactone)-*block*-poly(2-vinylpyridine) (PCL-*b*-P2VP) blends.[14] Ikkala et al.[15] investigated the morphology of blends of hexamethyltetramine-cured novolac with poly(2-vinylpyridine)-*block*-poly(isoprene) (P2VP-*b*-PI) and several other systems. In contrast, only few morphological studies[16,17] have involved complexes of a diblock copolymer and a homopolymer. Gohy et al.[16a] studied the micelle formation between polystyrene-*b*-poly(4-vinylpyridine) (PS-*b*-P4VP) copolymers and poly(acrylic acid) (PAA) homopolymers in organic solvents, where the micelle core consisted of neat PS. Jiang and co-workers[17c] investigated the micellization and stoichiometric complexation of PS-*b*-P4VP with formic acid (FA) in chloroform. Kwei et al.[18] reported the selective hydrogen bonding between the poly(*p*-hydroxystyrene) (PHS) block of PS-*b*-PHS diblock copolymer and poly(vinyl methyl ether) (PVME); however, they merely investigated the miscibility of PVME with both of the block copolymers at higher PVME contents based on DSC results. In all of these block copolymer/homopolymer complex systems, the hydrophobic PS block does not exhibit any specific interactions and miscibility with the other components (i.e., the homopolymer and the other block) and thus phase separates to give different microphase morphologies.

Here we report the results of an investigation into self-assembled solid-state complexes of poly(vinylphenol) (PVPh) and poly(ε-caprolactone)-*block*-poly(2-vinylpyridine) (PCL-*b*-P2VP). It is noted that PVPh is miscible with both PCL[19,20] and P2VP.[21] The phenol hydroxyls of PVPh have the capability to form hydrogen bonds with both the carbonyl groups of PCL and the pyridine nitrogen of P2VP. This system provides an example to investigate the competitive hydrogen bonding and its influence on the morphology in block copolymer/homopolymer complexes. This is an A-*b*-B/C type diblock copolymer/homopolymer system where C favorably interacts with both A and B. The interaction between different chains in an A-*b*-B/C type block copolymer/homopolymer system can be characterized

* Corresponding author: Tel +61 3 5227 2802; fax +61 3 5227 1103, e-mail qguo@deakin.edu.au.

10.1021/ma800703b CCC: $40.75
Published on Web 09/27/2008

by Flory−Huggins interaction parameter (χ). Here, the value of χ_{AB} is positive (A and B are immiscible) and χ_{AC}, χ_{BC} are negative, but $\chi_{BC} > \chi_{AC}$. The PVPh/PCL-*b*-P2VP complexes self-assemble into nanostructures due to the competition between the two blocks to form hydrogen bonds with the homopolymer. In this work, we investigate how hydrogen bonding determines the self-assembly and causes the formation of nanostructures in the PVPh/PCL-*b*-P2VP complexes. This work demonstrates how nanostructured complexes can be formed through the competitive hydrogen-bonding interactions.

The effect of hydrogen bonding on the phase behavior was investigated using differential scanning calorimetry (DSC) and Fourier transform infrared (FTIR) spectroscopy. The formation of complex aggregates in solution was investigated using dynamic light scattering (DLS). The semicrystalline morphology and microphase morphology of the complexes were examined using polarizing optical microscope (POM), atomic force microscope (AFM), transmission electron microscope (TEM), and small-angle X-ray scattering (SAXS).

Experimental Section

Materials and Preparation of Complexes. The polymers used in the present study were poly(4-vinylphenol) (PVPh) and poly(ε-caprolactone)-*block*-poly(2-vinylpyridine) (PCL-*b*-P2VP). PVPh is with an average $M_w = 20\,000$, obtained from Aldrich Chemical Co., Inc. The PCL-*b*-P2VP copolymer was from Polymer Source, Inc., with M_n(P2VP) = 20 900, M_n(PCL) = 26 100, and M_w/M_n = 1.11. The polymers were used as received.

The PVPh/PCL-*b*-P2VP complexes were prepared by solution mixing. Tetrahydrofuran (THF) solution containing 1% (w/v) of the individual polymers were mixed and stirred well until the complexes were precipitated. The solvent was allowed to evaporate slowly at room temperature. The samples were annealed under vacuum for 72 h before the measurements in order to reach equilibrium.

Differential Scanning Calorimetry (DSC). The thermal behavior of the complexes was analyzed by a Perkin-Elmer Diamond DSC. The measurement was performed using 5−10 mg of the sample under an atmosphere of helium gas. The samples were first heated to 100 °C and held at that temperature for 3 min to remove the thermal history. Then the samples were cooled to −50 °C at the rate of 20 °C/min, held for 5 min, and again heated from −50 to 200 °C at 20 °C/min. The glass transition temperature (T_g) was taken as the midpoint of transition, and the melting temperature (T_m) was taken as the maximum of the endothermic peak in the DSC thermograms.

Fourier Transform Infrared (FTIR) Spectroscopy. The KBr disk method was adopted to determine the FTIR characteristics of the complexes. The FTIR spectra of all the samples were measured on a Bruker Vetex 70 FTIR spectrometer. The THF sample solution was cast onto a KBr disk, and solvent was allowed to evaporate slowly at room temperature. The disks were dried under vacuum in an oven before taking the measurements. The spectra were recorded at the average of 32 scans in the standard wavenumber range of 400−4000 cm^{-1} at a resolution of 4 cm^{-1}.

Polarizing Optical Microscopy (POM). The morphology and semicrystalline morphology of PVPh/PCL-*b*-P2VP complexes were analyzed using a Nikon eclipse-80*i* optical microscope under polarized light. The THF cast solutions of the complex were spread as thin films on the glass slides and dried in a vacuum oven.

Dynamic Light Scattering (DLS). In DLS,[22] an autocorrelation function plots the average overall change in intensity with time, for a given time interval which is given by

$$G(\tau) = \int I(t)\, I(t+\tau)\, \mathrm{d}t \qquad (1)$$

where t is the delay time. In DLS all the information regarding the motion or diffusion of particles in the solution is embodied within the measured correlation curve, which can be fit to a single exponential form, i.e.

$$\int I(t)\, I(t+\tau)\, \mathrm{d}t = B + A \exp[-2q^2 D\tau] \qquad (2)$$

where B is the baseline, A is the amplitude, q is the scattering vector [$q = 4\pi\eta \sin(\theta/2)$, η is the refractive index of the solvent], and D is the diffusion coefficient.

The diffusion coefficient is calculated by fitting the correlation curve to an exponential function, with D being proportional to the exponential decay time. The hydrodynamic diameter (D_h) can be calculated using the particle diffusion coefficient and Stokes−Einstein equation given below, where k is the Boltzmann constant, T is the temperature, η is the refractive index, and h is the dispersant viscosity.

$$D_h = kT/3\pi\eta D \qquad (3)$$

DLS measurements were performed with a Malvern DLS spectrometer (Zetasizer Nano ZS) equipped with a He−Ne laser with a wavelength of 633 nm digital correlator. All measurements were carried out at 25 °C, with a detection angle of 173°. Solutions of 1% (w/v) complex aggregates in THF were used. The scattering intensity autocorrelation functions were analyzed by using the methods of CONTIN and cumulant which is based on an inverse Laplace transformation of the data and gives access to a size distribution histogram for the analyzed solutions.

Atomic Force Microscopy (AFM). The phase morphology of the complexes was examined using an AFM (DME type DS 45-40, Denmark) in the tapping mode at room temperature. The thin films of the samples were prepared by casting dilute solution of complexes on glass slides using a Laurell model WS-400B spin-coater operated at 3000 rpm. The samples were annealed under vacuum for 72 h before the measurements. The height and phase images were recorded simultaneously while operating the instrument in the tapping mode.

Small-Angle X-ray Scattering (SAXS). The SAXS measurements were performed with a Bruker NanoSTAR SAXS instrument at room temperature. Samples having 1 mm thickness were prepared for SAXS measurements. Two-dimensional diffraction patterns collected were subtracted from background scattering, corrected, and converted into one-dimensional format (intensity vs scattering wave vector q) by azimuthal averaging of the data [$q = (4\pi/\lambda) \sin(\theta/2)$, where $\lambda = 0.154$ nm is the scattering wavelength and θ is the scattering angle].

Transmission Electron Microscopy (TEM). TEM experiments were performed on a JEOL JEM-2100 transmission electron microscope at an acceleration voltage of 80 kV. A drop of the dilute solution was placed onto a carbon-coated TEM copper grid. The excess solution was blotted away using a strip of filter paper after 2 min. The samples were allowed to dry at room temperature and then stained by ruthenium tetroxide.

Results and Discussion

Formation of PVPh/PCL-*b*-P2VP Complexes. PVPh forms complexes with poly(vinylpyridine)s.[23,24] Lee et al.[25] investigated the hydrogen-bonding interactions in PVPh/P2VP complexes formed in THF. Zhao et al.[26] conducted X-ray photoelectron spectroscopic measurements on complexes obtained from PVPh and P2VP or P4VP. The complexation between poly(styrene-*co*-vinylphenol) (STVPh) and poly(styrene-*co*-vinylpyridine) (STVPy) in THF solution was investigated by Xiang et al.[27] with emphasis on the effect of the hydroxyl and pyridyl contents in the component polymers. PVPh and PCL-*b*-P2VP formed a complex in THF which was confirmed by the immediate precipitation (as shown in Figure 1) due to the network formation when 1% (w/v) solution of the two polymers mixed together. The important factors governing the formation of complex are the specific interaction between the component polymers and the solvent medium in which complex formation

Figure 1. Photograph of 50/50 PVPh/PCL-*b*-P2VP complex formed in 1% (w/v) tetrahydrofuran (THF) solution.

takes place. This is because the solvent molecules can also act as either hydrogen donor or hydrogen acceptor and thereby take part in the hydrogen bonding between the component polymers.[28] Since THF is an aprotic solvent, it can interact favorably with proton donating polymers such as PVPh. In the present system, the extent of hydrogen-bonding interaction between PVPh and PCL-*b*-P2VP is superior to the interaction between PVPh and the solvent, which leads to the formation of complex. Complexes will not form if the solvent is able to interact strongly with one or both of the polymers. For example, PVPh forms complexes with P2VP and with P4VP in ethanol or THF but not in *N,N*-dimethylformamide (DMF).[24a]

The formation of complex aggregates in solution was examined using DLS. Figure 2 illustrates the intensity distributions of apparent hydrodynamic diameter (D_h) of the PVPh/PCL-*b*-P2VP complex aggregates in 1% (w/v) THF solutions. The DLS data of pure PCL-*b*-P2VP are also given for comparison. For each complex solution, the hydrodynamic diameter distribution consists of a single peak with a narrow distribution. It can be noted that the peak of the complexes shifts toward higher D_h with increasing PVPh content. While the pure PCL-*b*-P2VP gives the peak position of D_h at 20 nm, the complex solutions exhibit much larger D_h values from 46 to 72 nm with PVPh content from 10 to 50 wt %. This is obviously due to the swelling of the block copolymer by both PVPh homopolymer and solvent THF. Micelles with different size distributions are formed in the solution at different complex compositions. The peaks at lower PVPh concentrations (10 and 20 wt % PVPh) exhibit a narrow profile, which means that the micelles formed have a low polydispersity. With increasing PVPh concentration from 30 to 50 wt %, the size of the microphases and its distribution significantly increase, which can be identified by the broadening of the DLS peaks. It should be pointed out that DLS measurements provide only apparent D_h values and do not give information about the true shape of the micelles.[22]

Competitive Hydrogen-Bonding Interactions in PVPh/PCL-*b*-P2VP Complexes. FTIR characterization was intended to investigate the specific interactions in the PVPh/PCL-*b*-P2VP complexes. Figure 3 summarizes the possible hydrogen-bonding interactions in the complex. The hydroxyl stretching region in the infrared spectrum of PVPh/PCL-*b*-P2VP complex is susceptible to hydrogen-bonding interactions, which is given in Figure 4. The hydroxyl region of pure PVPh consists of two bands: a broad band centered at 3350 cm^{-1} corresponding to the absorption of self-associated hydroxyl groups and a relatively narrow band at 3525 cm^{-1} corresponding to the free hydroxyl groups.[20] In the figure the free hydroxyl absorption band appears as a shoulder, which indicates that relatively smaller amount of free hydroxyl groups are present compared with the widely distributed self-associated hydroxyl groups. The free hydroxyl band does not shift, but its intensity decreases and eventually disappears as the concentration of the PCL-*b*-P2VP block copolymer increases in the complex, which indicates that the hydroxyl groups of PVPh are hydrogen bonded with pyridine nitrogens and carbonyl groups.

In contrast, the associated hydroxyl band at 3350 cm^{-1} shifts to higher frequencies with increasing PCL-*b*-P2VP concentration, indicating that there is hydrogen bonding between the hydroxyl groups of PVPh and the carbonyl groups of PCL block. The frequency difference between the free hydroxyl absorption and that of the hydrogen-bonded species ($\Delta\nu$) is a measure of the average strength of the interactions.[29−31] Therefore, this shift indicates that the average strength of the hydrogen bond between the hydroxyl groups of PVPh and the carbonyl groups of PCL block in the complexes ($\Delta\nu = 85$ cm^{-1} for 20/80 PVPh/PCL-*b*-P2VP complex) is much lower than that between the hydroxyl groups in the pure PVPh ($\Delta\nu = 175$ cm^{-1}). Similar results have been observed by other investigators[31−33] for PCL with PVPh and other polymers containing hydroxyl groups. It is noted that the a new hydroxyl stretching band appears around 3195 cm^{-1} in the complexes with 20 and 40 wt % PVPh. This hydroxyl stretching band observed in the complexes with low PVPh concentrations can be plausibly assigned to the hydrogen-bonding interaction between hydroxyl groups of PVPh and pyridine nitrogens of P2VP ($\Delta\nu = 330$ cm^{-1}), which is remarkably stronger than that between the hydroxyl groups in the pure PVPh ($\Delta\nu = 175$ cm^{-1}).

To further confirm the hydrogen-bonding interactions in the complex, the carbonyl stretching region, ranging from 1650 to 1790 cm^{-1}, of the PVPh/PCL-*b*-P2VP complexes at room temperature is given in Figure 5. The two carbonyl bands of pure PCL-*b*-P2VP, one relatively sharp at 1725 cm^{-1} and the other seen as a shoulder at 1734 cm^{-1}, can be attributed to crystalline and amorphous conformations of PCL, respectively.[34] As the concentration of PVPh is increased in the complex, another band at 1710 cm^{-1} is observed which increases in relative intensity with increasing PVPh content. This band is due to the vibration of the hydrogen-bonded PCL carbonyl groups. It can be noticed that the intensity of the hydrogen-bonded carbonyl band increases very slowly with increase in PVPh content compared to the free carbonyl band. Hence, it can be concluded that the fraction of hydrogen-bonded carbonyl groups is relatively less in the PVPh/PCL-*b*-P2VP complexes at lower PVPh concentrations. This is obviously due to the presence of P2VP component in the block copolymer which can form strong hydrogen bonds with PVPh hydroxyl groups.[35]

The hydrogen-bonding ability of carbonyl groups was also investigated at 75 °C, above the melting point of PCL. Figure 6 shows the IR spectra of carbonyl stretching region ranging from 1660 to 1800 cm^{-1} at 75 °C for PVPh/PCL-*b*-P2VP complexes. The pure PCL-*b*-P2VP block copolymer shows a single peak at 1734 cm^{-1} corresponding to the amorphous conformations of PCL. For complexes, two bands can be observed in the carbonyl stretching region corresponding to the free carbonyl groups (1734 cm^{-1}) and the hydrogen-bonded carbonyl (1710 cm^{-1}) groups. The crystalline peak which was observed at 1725 cm^{-1} in the carbonyl region at room temperature (Figure 5) is not visible here because of the melting of the crystalline component of PCL at 75 °C. In general, the number of hydrogen bonds for a given system decreases with increasing temperature due to the negative enthalpy of hydrogen bond formation. On the other hand, the number of hydrogen bonds formed with crystalline/semicrystalline polymer may

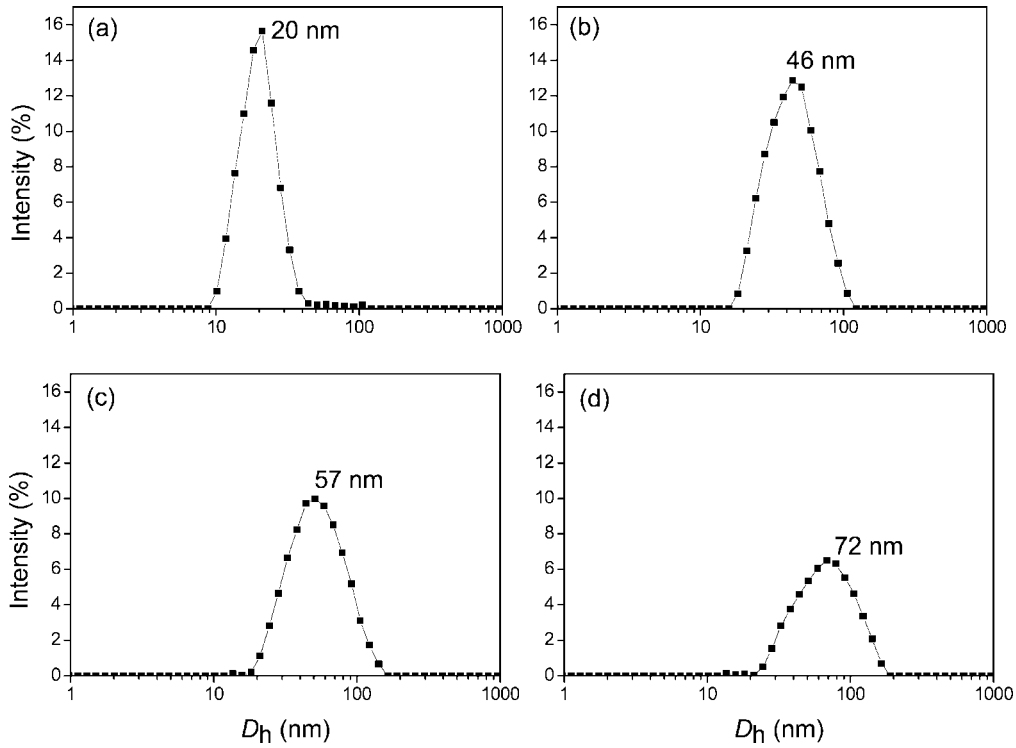

Figure 2. Hydrodynamic diameter (D_h) distribution of (a) 0/100, (b) 10/90, (c) 30/70, and (d) 50/50 PVPh/PCL-*b*-P2VP complex aggregates in 1% (w/v) tetrahydrofuran (THF) solutions.

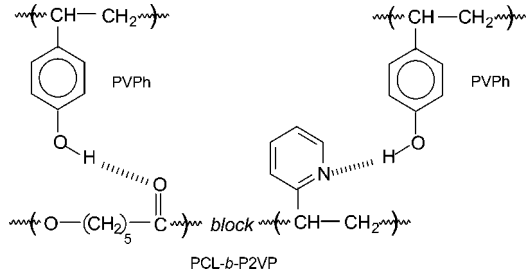

Figure 3. Schematic representation of possible interactions between PVPh and PCL-*b*-P2VP block copolymer.

increase with increasing temperature as the crystalline phase melts progressively.

In addition to hydroxyl and carbonyl stretching regions, some characteristic bands of pyridine ring are sensitive to hydrogen-bonding interaction. The most affected bands for P2VP are those concerned with stretching modes of pyridine ring at 1590 and 993 cm^{-1}. These bands arise from the changes in the electronic distribution in the pyridine ring due to the formation of hydrogen bonds. The band at 1590 cm^{-1} becomes broad and shifts toward higher wavenumbers as the PVPh content increases in the complex, which is due to the increase in stiffness of the pyridine ring as a result of hydrogen bonding.[36] The infrared spectra corresponding to this region are shown in Figure 7. Pure PVPh exhibits an absorption band at 1013 cm^{-1}. Another absorption band can be observed in the PVPh/PCL-*b*-P2VP complexes at 1005 cm^{-1}, which can be attributed to the hydrogen-bonding interaction between pyridine ring of P2VP and phenol group of PVPh. The infrared spectra corresponding to this region are shown in Figure 8. The interaction between pendant pyridine groups of P2VP and phenol group of PVPh is very significant in the formation of a stable complex between these polymers. This hydrogen bonding can contribute much to the positive deviation of T_g observed in the DSC T_g−composition plot of the complex which is described in the later part of this article.

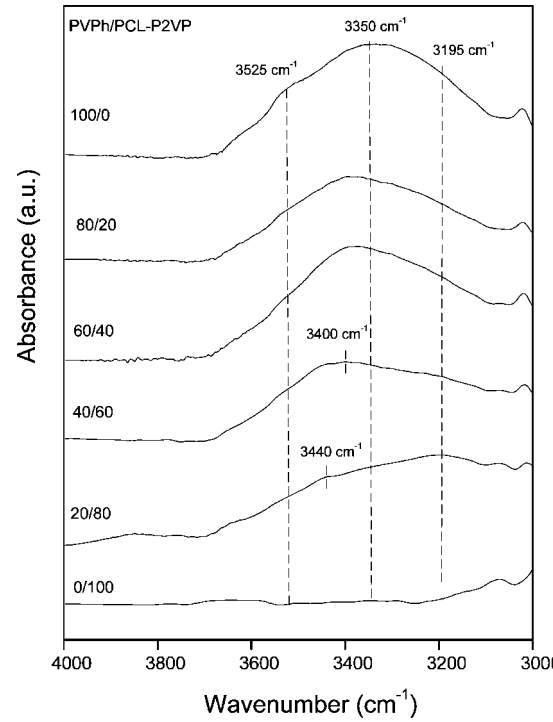

Figure 4. Hydroxyl stretching region in the infrared spectra of PVPh/PCL-*b*-P2VP complexes.

The quantitative study of fraction of hydrogen-bonded carbonyl groups and pyridine groups can be performed with the variation in composition. The fraction of hydrogen-bonded carbonyl groups and hydrogen-bonded pyridine groups can be calculated using the equation

$$f_b = \frac{A_b/a}{A_b/a + A_f} \tag{4}$$

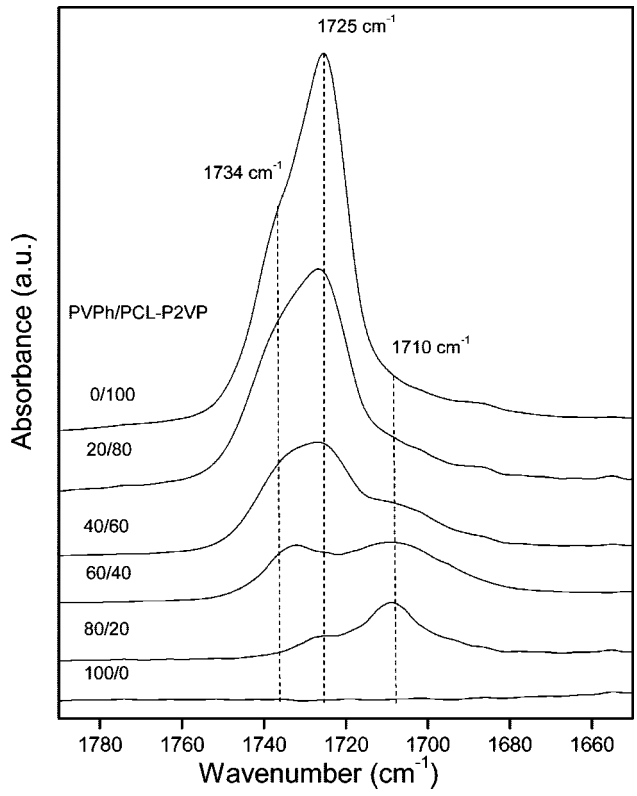

Figure 5. Carbonyl stretching region of PVPh/PCL-*b*-P2VP complexes at room temperature.

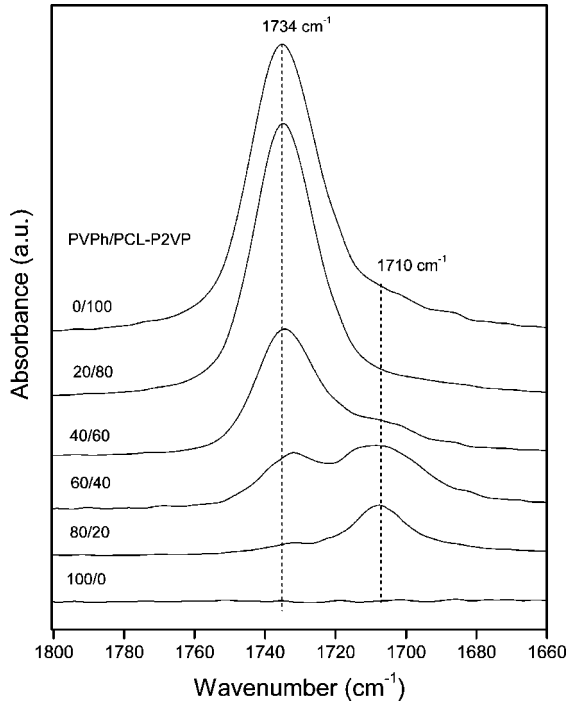

Figure 6. Carbonyl stretching region of PVPh/PCL-*b*-P2VP complexes at 75 °C.

A_f and A_b are the peak areas of the free and hydrogen-bonded carbonyl/pyridine groups. The conversion constant a is the specific absorption ratio of the above two bands. The value of $a = 1.5$ for the PVPh/PCL system and $a = 1$ for PVPh/P2VP, which were determined previously.[34,36] The results from curve fitting at room temperature are summarized in Tables 1 and 2. These results indicate that the fraction of hydrogen-bonded carbonyl/pyridine groups increase with increase in the PVPh content. The fraction of hydrogen-bonded carbonyl groups is relatively small compared to the fraction of hydrogen-bonded pyridine groups at low PVPh concentrations.

From the FTIR data given in Figure 5 and Table 1, it can be noticed that, up to 40 wt % of PVPh, the peak intensity and

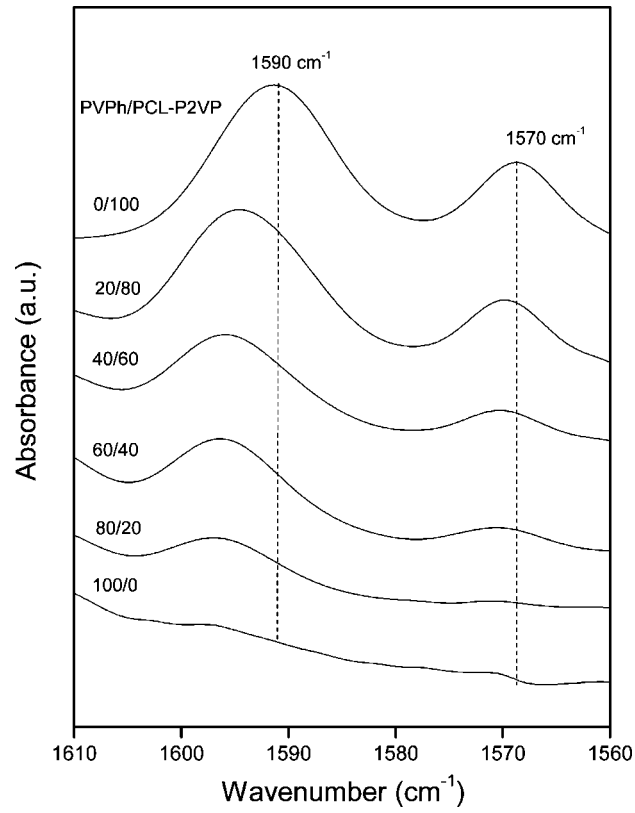

Figure 7. Infrared spectra corresponding to the wavenumber region of 1560−1610 cm^{-1} of different PVPh/PCL-*b*-P2VP complexes at room temperature.

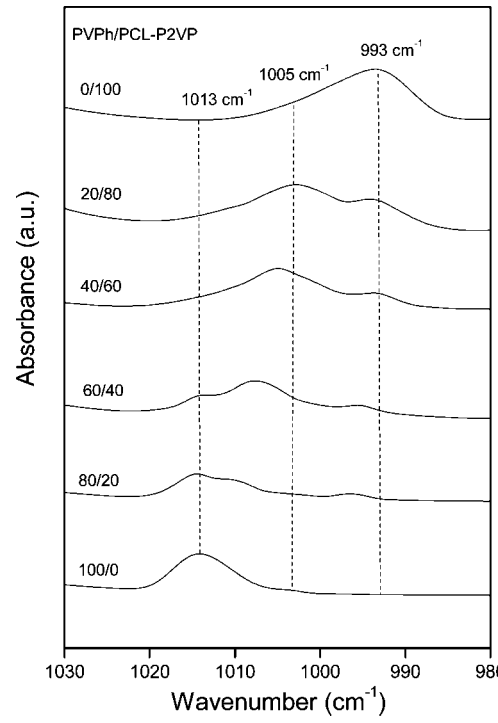

Figure 8. Infrared spectra corresponding to the wavenumber region of 980−1020 cm^{-1} of different PVPh/PCL-*b*-P2VP complexes at room temperature.

Table 1. Curve-Fitting Results of PVPh Hydroxyl and PCL Carbonyl Interactions in PVPh/PCL-*b*-P2VP Complexes at Room Temperature

	amorphous C=O			crystalline C=O			bonded C=O			
PVPh/PCL-*b*-P2VP	υ (cm^{-1})	$W_{1/2}$ (cm^{-1})	A_a (%)	υ (cm^{-1})	$W_{1/2}$ (cm^{-1})	A_c (%)	υ (cm^{-1})	$W_{1/2}$ (cm^{-1})	A_b (%)	f_b (%)
80/20	1734.2	11.57	37.1				1704.5	31.30	62.9	53.05
60/40	1734.8	12.31	57.9				1705.9	29.27	42.1	32.65
40/60	1735.1	13.89	48.87	1724.3	14.2	36.23	1706.1	24.63	14.9	16.90
20/80	1735.8	15.79	29.74	1724	9.8	62.56	1706.8	22.36	3.7	7.68

Table 2. Curve-Fitting Results of PVPh Hydroxyl and P2VP Pyridine Interactions in PVPh/PCL-*b*-P2VP Complexes at Room Temperature

	free pyridine group			bonded pyridine group			
PVPh/PCL-*b*-P2VP	υ (cm^{-1})	$W_{1/2}$ (cm^{-1})	A_f (%)	υ (cm^{-1})	$W_{1/2}$ (cm^{-1})	A_b (%)	f_b (%)
80/20	1570.1	12.97	11.1	1597.5	18.26	88.9	88.9
60/40	1570.6	11.52	19.34	1596.1	17.56	80.66	80.66
40/60	1570.8	8.38	41.1	1595.3	17.89	58.9	58.9
20/80	1570.4	7.30	60.21	1594.4	16.98	39.79	39.79

fraction of the hydrogen-bonded carbonyl groups are relatively less compared to the free carbonyl peak. The carbonyl groups of PCL block are less involved in hydrogen bonding in the present complex system compared with the PVPh/PCL binary blends investigated by other authors.[35] In the present PVPh/PCL-*b*-P2VP complexes, PCL block forms hydrogen bonds with PVPh, and the average strength of these bonds increases with increasing PVPh concentration. The PCL block exhibits strong hydrogen bonding with PVPh only when PVPh content reaches 60 wt %. This is due to the competitive hydrogen-bonding interaction between PVPh/P2VP blocks and PVPh/PCL blocks. Since the ability of P2VP to form hydrogen bonds with PVPh is relatively high compared with PCL, the P2VP blocks form high degree of bonding with PVPh.

Phase Behavior and Semicrystalline Morphology. The thermal properties of PVPh/PCL-*b*-P2VP complexes were analyzed using DSC. The DSC thermograms for the heating scan after the cooling of PVPh/PCL-*b*-P2VP complexes with various compositions are shown in Figure 9.

The pure block copolymer was expected to exhibit two glass transition temperatures (T_gs) corresponding to the PCL blocks and P2VP blocks, respectively. In PVPh/PCL-*b*-P2VP mixture, since PVPh is miscible with both blocks, a reduction in T_g of both components was expected, whereas a single T_g corresponding to the PVPh and P2VP components was detected. This can be attributed to the formation of strong intermolecular interaction between P2VP and PVPh. The T_g corresponding to the PCL blocks was not discernible from the DSC curves under the experimental conditions.

The T_g−composition plot corresponding to PVPh/P2VP phase is shown in Figure 10. It can be observed that the positive deviation from the linearity rule is obvious in the T_g−composition plot. The main factor for such a positive deviation is the strong hydrogen-bonding interaction between the component polymers. The Kwei equation[37] is generally used for discussing the glass transition behavior of polymer mixtures with specific interactions. The Kwei equation is given as follows: where W_1 and W_2 are the weight fractions of the components

$$T_g = \frac{W_1 T_{g1} + qW_2 T_{g2}}{W_1 + kW_2} + qW_1 W_2 \quad (5)$$

in the complexes, T_{g1} and T_{g2} represent the corresponding glass

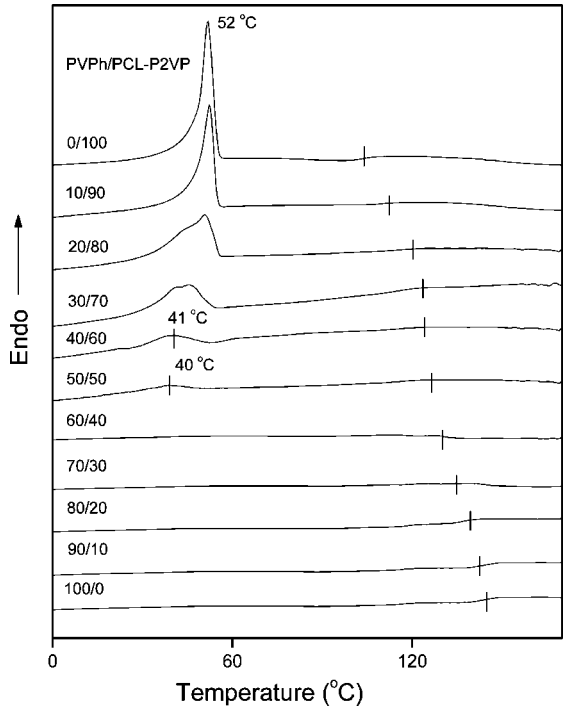

Figure 9. DSC curves of PVPh/PCL-*b*-P2VP complexes with different PVPh concentrations.

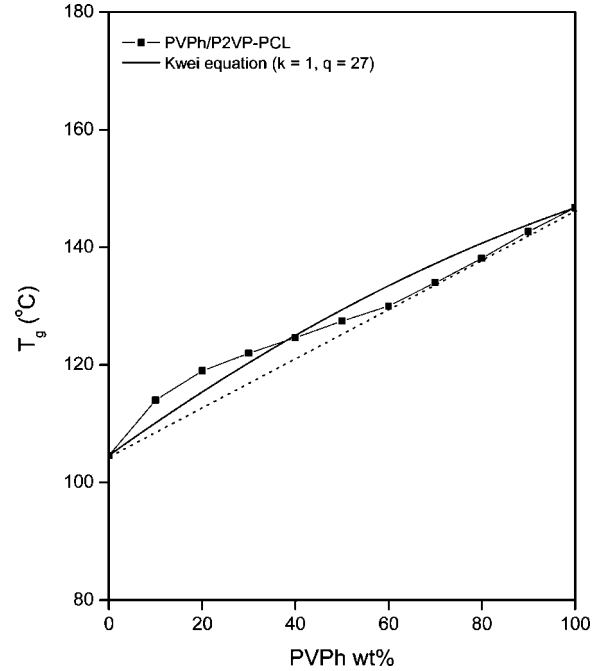

Figure 10. T_g−composition relationship of PVPh/PCL-*b*-P2VP complexes.

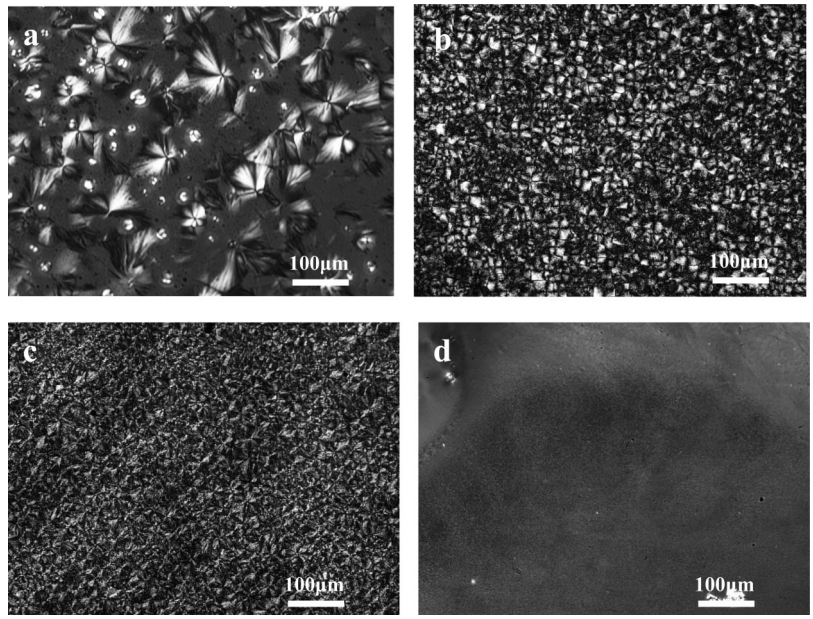

Figure 11. POM morphologies of different PVPh/PCL-*b*-P2VP complexes at room temperature. PVPh/PCL-*b*-P2VP: (a) 0/100, (b) 10/90, (c) 20/80, and (d) 30/70.

transition temperatures, and k and q are the fitting parameters which can be obtained from the least-squares best fit values. Here, q is the parameter corresponding to the strength of hydrogen bonding in the blend and is considered as the balance between the breaking of the self-association hydrogen bonding and the forming of interassociation. The fitting leads to a result of $k = 1$ and $q = 27$ for the PVPh/PCL-*b*-P2VP system. In this study a positive q value is obtained, indicating a strong interaction between the PVPh and PCL-*b*-P2VP copolymer.[38]

The melting point depression is an important characteristic of polymer mixtures where intermolecular interactions exist.[39] The melting point depression is more profound in polymer complexes owing to stronger interactions. The melting point depression of the crystalline component in a mixture provides significant information about its miscibility behavior and intermolecular interactions. The reduction in temperature is caused by the thermodynamic changes due to the reduction in the chemical potential. When two polymers are miscible in the melt, the chemical potential of the crystallizable polymer is decreased due to the addition of the second component. This is the reason for the reduction in equilibrium melting temperature upon the addition of the amorphous component. It is believed that the melting point depression is larger in hydrogen-bonded polymer mixtures. But here from Figure 9, it can be predicted that, though the intensities of melting peaks corresponding to PCL crystalline phase decreases with increase in content of PVPh, the melting point (T_m) decreases slowly or at low PVPh contents. From the above results, it can be concluded that the intermolecular hydrogen-bonding interaction between PCL blocks and PVPh becomes very stronger after 60 wt % of PVPh. This is due to the more favored formation of hydrogen bonds between PVPh and P2VP rather than between PVPh and PCL. These results are entirely consistent with the FTIR results described above.

The semicrystalline morphology of the PVPh/PCL-*b*-P2VP complexes was examined using the optical microscopy. The THF cast films were analyzed at different magnifications. The polarizing optical microscopic (POM) images are given in Figure 11. From the figure it is clear that the pure PCL-*b*-P2VP block copolymer contains PCL crystalline spherulites. As the concentration of PVPh increases in the complexes, the spherulites become smaller and eventually disappear. The complexes containing 30 wt % or above PVPh have no clear indication of crystalline structures, which indicates that the PCL fractions were constrained from crystallization under the experimental conditions.

Self-Assembly and Nanostructures in PVPh/PCL-*b*-P2VP Complexes. Binary mixtures of block copolymers with homopolymers can form a rich variety of microstructures which are the result of the spontaneous interfacial areas and curvatures that are established at equilibrium.[40] The average interfacial curvature is highest for spheres and decreases progressively toward planar interfaces in lamellae. In a system containing a diblock copolymer A-*b*-B and a homopolymer C, and A rather than B is strongly solubilized by C, B can form microdomains depending on the concentration. The interface of spherical microdomains consists of the copolymer segment B as the core and the copolymer segment A solubilized by homopolymer C as the corona.[41]

The microphase-separated morphology of the complexes was examined using AFM. The AFM images of the pure block copolymer and PVPh/PCL-*b*-P2VP complexes are given in Figure 12. The left and right images are the height and phase images, respectively. The morphology of the pure PCL-*b*-P2VP block copolymer is given in Figure 12a, which displays some characteristics of an ordered microphase-separated structure with average size of about 20 nm. The SAXS results shown in Figure 14 reveal that the pure PCL-*b*-P2VP block copolymer exhibits a hexagonally packed cylindrical morphology. Upon the addition of PVPh, which selectively swells the block copolymer, different morphologies can be observed. In the 10 wt % PVPh complex, spherical micelles (Figure 12b) having diameter in the range of 30−40 nm were obtained. The shape of the micelles changes with increasing PVPh concentration, displaying characteristics of elongated micelles in 30 wt % PVPh complex (Figure 12c). Wormlike micelles with size in the order of 40−50 nm in diameter can be clearly observed in 50 wt % PVPh complex (Figure 12d). As the concentration further increases, the microdomains disappear as seen in 80 wt % PVPh complex (Figure 12e).

The formation of the microdomains can be attributed to the exclusion of weakly associated PVPh/PCL phase that has been separated from the mixed phase where P2VP forms strong

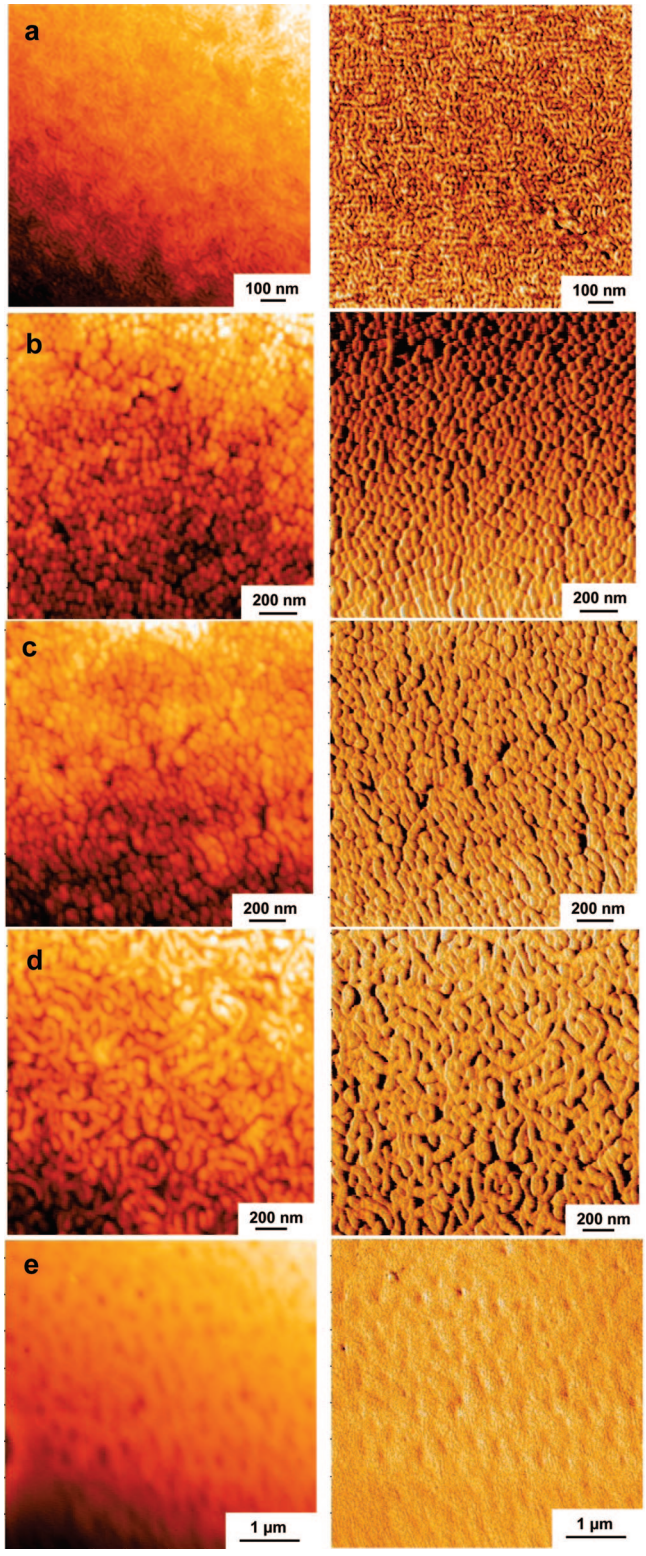

Figure 12. AFM images of (a) 0/100, (b) 10/90, (c) 30/70, (d) 50/50, and (e) 80/20 PVPh/PCL-*b*-P2VP complexes. Left: height image; right: phase image.

association with PVPh. At low PVPh content, PVPh and the P2VP block form a single phase. With increasing PVPh concentration, the PCL block also forms hydrogen bonds with PVPh, which results in a nonuniform distribution of PVPh in the core and corona. In 30−60 wt % PVPh complexes, the cores of the micelles consist of PVPh/PCL single phase due to the intermolecular hydrogen bonding between PVPh and the PCL block. This causes a decrease in the interfacial area and the

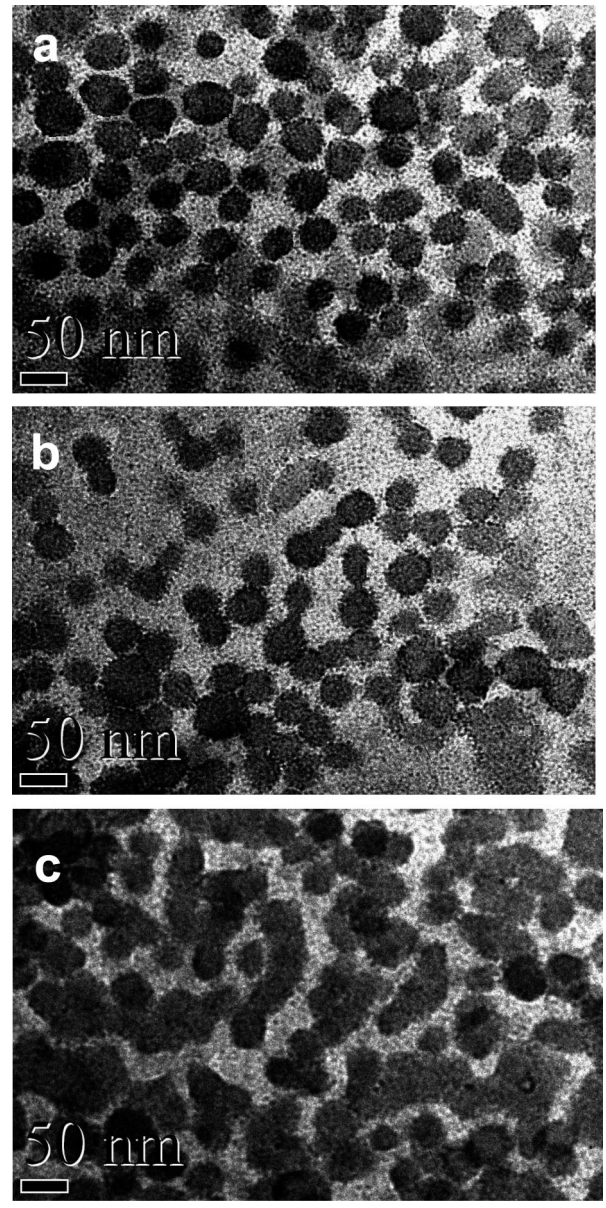

Figure 13. TEM picture of (a) 10/90, (b) 30/70, and (c) 50/50 PVPh/PCL-*b*-P2VP complexes.

morphology changes from spherical micelles to wormlike micelles.[41] On further increasing the PVPh content (70 wt % or above), the carbonyl groups in the PCL blocks interact even more strongly with PVPh hydroxyl groups, resulting in a homogeneous phase containing three components. This result confirms those observed by DSC and FTIR studies explained earlier.

TEM was also performed to investigate the morphologies of the complexes as illustrated in Figure 13. TEM results give an unambiguous picture of the morphological transformations in these complexes. It can be observed that spherical microdomains are obtained in 10 wt % PVPh complexes as shown in Figure 13a. The size of the microdomains is approximately 25−35 nm. The spherical microdomains are interconnected in 30 wt % PVPh complexes as shown in the Figure 13b. This can be considered as the commencement of formation of elongated structures like wormlike or rodlike microdomains. As the concentration of PVPh increases, it is found that the complex forms wormlike micelles. Wormlike morphology obtained in 50 wt % PVPh complexes is shown in Figure 13c. It can be assumed that this wormlike morphology exists in 30−50 wt %

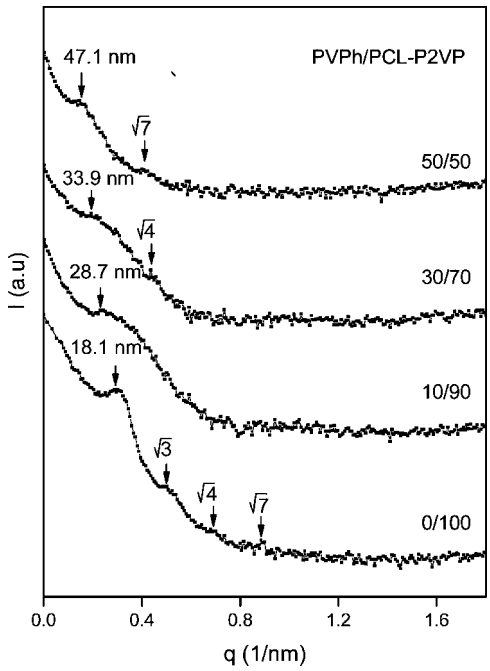

Figure 14. SAXS profiles of PVPh/PCL-*b*-P2VP complexes.

PVPh complexes as also observed in AFM experiments (Figure 12). However, above 70 wt % PVPh complexes show no particular morphology (not given), which suggests a homogeneous system in these complexes. The TEM observation is in agreement with the AFM results.

SAXS profiles of PVPh/PCL-*b*-P2VP complexes were taken at room temperature in order to confirm the microphase-separated morphology and are shown in Figure 14. For pure PCL-*b*-P2VP block copolymer, the first-order scattering peak corresponds to a Bragg spacing of a spacing of 18.1 nm, which is the average spacing between the PCL and neighboring P2VP microphases. The peak positions in the SAXS profile indicate of hexagonally packed cylindrical morphology, i.e., $q/q^* = \sqrt{1}:\sqrt{3}:\sqrt{4}:\sqrt{7}...$ (where q^* denotes the position of the first-order scattering maximum).[40,42] The complexes give broad peaks, and the broadening of the peak indicates the absence of long-range ordered structures. However, 30 and 50 wt % PVPh complexes show another small peak around $\sqrt{4}$ and $\sqrt{7}$, respectively, owing to the incomplete disordering of the hexagonal cylinders present in the complexes. The SAXS profile of 10 wt % PVPh complex displays characteristics of spherical micelles. The average spacing between the neighboring microdomains increases in the order 28.7, 33.9, and 47.1 nm for 10, 30, and 50 wt% PVPh/PCL-*b*-P2VP complexes. From the whole shapes of the SAXS profiles in Figure 14, it can be concluded that there exists only short-range ordered nanostructures in PVPh/PCL-*b*-P2VP complexes.

On the basis of FTIR, DSC, AFM, TEM, and SAXS results reported above, a possible model for the microphase structure in the PVPh/PCL-*b*-P2VP complexes could be postulated and is shown in Figure 15. The complex system contains an immiscible block copolymer P2VP-*b*-PCL and a homopolymer PVPh that is miscible with both the PCL and P2VP blocks. Figure 14a shows a schematic representation of PVPh/PCL-*b*-P2VP complex with 10 wt % PVPh where spherical micelles are formed. Here, PVPh and the P2VP block interact very strongly to form one single phase as the corona of special micelle. The PCL block is immiscible with the P2VP block and weakly associates with PVPh. The core of spherical micelle is composed of a PCL microdomain at the center surrounded by PVPh/P2VP single phase, as shown in Figure 14a. The average size of these spherical micelles is 30−40 nm in diameter. In the complexes containing 30−60 wt % of PVPh, both the PCL and P2VP blocks are swollen by PVPh. The structure of these micelles changes as shown in Figure 14b, which is as a result of the formation of a PVPh/PCL single phase in the complex due to the non-negligible hydrogen bonding between PVPh and PCL. The formation of the PVPh/PCL single phase causes a decrease in the interfacial area, which results in the planar interfaces and thereby the formation of wormlike micelles with size in the order of 40−50 nm. When the concentration of PVPh further increases, the PCL block starts interacting strongly with PVPh, and a homogeneous phase containing all the three-component polymers appears as schematically represented in Figure 14c.

The observed morphological changes can be explained in terms of the hydrogen-bonding ability of PVPh with the PCL block at high PVPh concentrations. Since the fraction of free hydroxyl groups which are available for hydrogen bonding is large at higher PVPh contents, the PCL block can easily form intermolecular hydrogen bonds with PVPh. This results in the homogeneous phase consisting of PVPh, PCL, and P2VP as shown in Figure 14c. At lower PVPh concentration, the nanostructures in the complex are formed by the competitive interactions between the block copolymer blocks and the homopolymer PVPh. At higher concentrations, PVPh homopolymer can act as a nonselective polymer solvent for both of the blocks. That is, when the PVPh content is above 60 wt %, it can act as a common solvent for both of the blocks which results in a homogeneous complex.

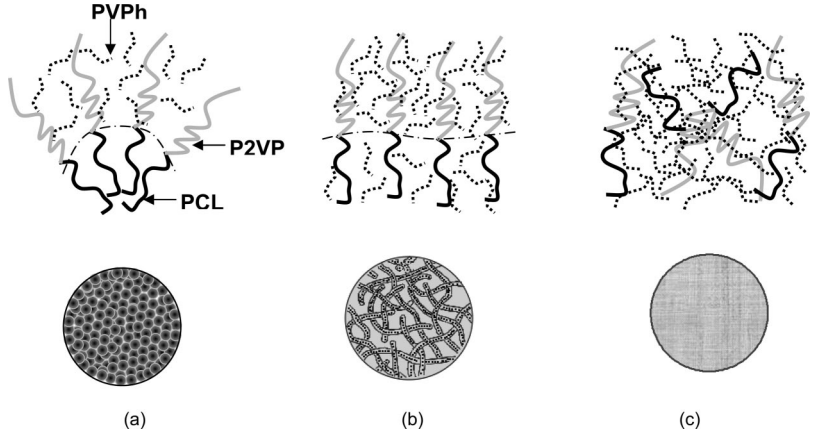

Figure 15. Schematic representation of different phase behavior in PVPh/PCL-*b*-P2VP complexes: (a) spherical micelles at 10 wt % PVPh concentration, (b) wormlike micelles at 30−60 wt % PVPh concentration, and (c) homogeneous at 80 wt % PVPh concentration.

In PVPh/PCL-*b*-P2VP complexes a completely homogeneous system could be expected since it has been proved that both PCL and P2VP form homogeneous binary mixtures with PVPh. However, the competitive hydrogen-bonding interaction between P2VP/PVPh and PCL/PVPh pairs resulted in the formation of nanostructured complexes since PCL fails to form strong hydrogen bonds with PVPh at lower homopolymer concentrations. That is, PCL, which is completely miscible with PVPh in binary blends, is enforced to phase separate and forms nanostructures due to the strongly hydrogen-bonded P2VP/PVPh pair. Hence, it can be proposed that nanostructures can be created in such systems where competitive hydrogen-bonding interactions between the blocks differ significantly.

Conclusions

We have investigated the formation of nanostructured complexes between PCL-*b*-P2VP block copolymer and PVPh homopolymer due to the existence of two different types of hydrogen bonding. PVPh hydroxyl group can selectively interact with both pyridine group of P2VP and carbonyl group of PCL, which leads to the formation of nanostructures in the present complex system. The competitive hydrogen bonding between PVPh/P2VP pair and PVPh/PCL pair resulted in the formation of composition-dependent nanostructures in the complexes. The FTIR results provide clear evidence for the formation of hydrogen bonds in this complex system. The hydrogen-bonding interaction between PVPh and P2VP block is significantly stronger than that between PVPh and PCL block. The positive deviation observed in the T_g−composition plot confirms that strong specific interactions exist in the present system. The morphological studies elucidate that the crystalline PCL blocks become more and more soluble as the PVPh content increases in the complex. PCL-*b*-P2VP microphase separates as both P2VP block and PCL block selectively interact with PVPh at low PVPh contents. The complexes are nanostructured and exhibit morphological transformation from spherical to wormlike micelles, dependent on the composition. The microphase-separated morphology eventually disappears and leads to a homogeneous complex with 80 wt % PVPh. The formation of nanostructures can be attributed to the competitive hydrogen-bonding interactions in the system.

Acknowledgment. This work was financially supported by the Australian Research Council under the Discovery Projects Scheme and by Deakin University through a CRGS grant. N.H. expresses his gratitude for a DUIRS scholarship from Deakin University. The authors thank Dr. Pavel Cizek, Deakin University, for TEM experimental support.

References and Notes

(1) (a) Brinke, G.; Ruokolainen, J.; Ikkala, O. *Adv. Polym. Sci.* **2007**, *207*, 113. (b) Bates, F. S.; Fredrickson, G. H. *Phys. Today* **1999**, *52*, 33. (c) MolauG. E. *Colloidal and Morphological Behaviour of Block Copolymers*; Molau, G. E., Ed.; Plenum Press: New York, 1971. (d) Mogi, Y.; Nomura, M.; Kotsuji, H.; Ohnishi, K.; Matsushita, Y.; Noda, I. *Macromolecules* **1994**, *27*, 6755. (e) Gido, S. P.; Schwark, D. W.; Thomas, E. L.; Goncalves, M. C. *Macromolecules* **1993**, *26*, 2636. (f) Stadler, R.; Auschra, C.; Beckmann, J.; Krappe, U.; Voigt-Martin, I.; Leibler, L. *Macromolecules* **1995**, *28*, 3080. (g) Gohy, J. F. *Adv. Polym. Sci.* **2005**, *190*, 65. (h) Hu, Z.; Jonas, A. M.; Varshney, S. K.; Gohy, J. F. *J. Am. Chem. Soc.* **2005**, *127*, 6526. (i) Zhang, G.; Liu, S.; Zhao, H.; Jiang, M. *Mater. Sci. Eng., C* **1999**, *10*, 155. (j) Mu, M.; Ning, F.; Jiang, M.; Chen, D. *Langmuir* **2003**, *19*, 9994.
(2) Zoelen, W.; Ekenstein, G. A.; Ikkala, O.; Brinke, G. *Macromolecules* **2006**, *39*, 6574.
(3) Huang, Y. M.; Liu, H. L.; Hu, Y. *Macromol. Theory Simul.* **2006**, *15*, 321.
(4) Huang, Y. Y.; Chen, H. L.; Hashimoto, T. *Macromolecules* **2003**, *36*, 764.
(5) Huang, Y. Y.; Hsu, J. Y.; Chen, H. L.; Hashimoto, T. *Macromolecules* **2007**, *40*, 3700.
(6) Matsushita, Y. *Macromolecules* **2007**, *40*, 771.
(7) Vaidya, N. Y.; Han, C. D. *Polymer* **2002**, *43*, 3047.
(8) Jiang, M.; Xie, H. *Prog. Polym. Sci.* **1991**, *16*, 977.
(9) Nobuhiro, N.; Kazunori, K. *Adv. Polym. Sci.* **2006**, *193*, 67.
(10) Antonietti, M.; Conrad, J.; Thünemann, A. *Trends. Polym. Sci.* **1997**, *5*, 262.
(11) Mogi, Y.; Nomura, M.; Kotsuji, H.; Ohnishi, K.; Matsushita, Y.; Noda, I. *Macromolecules* **1994**, *27*, 6755.
(12) Gido, S. P.; Schwark, D. W.; Thomas, E. L.; Goncalves, M. C. *Macromolecules* **1993**, *26*, 2636.
(13) Stadler, R.; Auschra, C.; Beckmann, J.; Krappe, U.; Voigt-Martin, I.; Leibler, L. *Macromolecules* **1995**, *28*, 3080.
(14) Hameed, N.; Guo, Q. *Polymer* **2008**, *49*, 922.
(15) (a) Kosonen, H.; Ruokolainen, J.; Nyholm, P.; Ikkala, O. *Macromolecules* **2001**, *34*, 3046. (b) Ruokolainen, J.; Mäkinen, R.; Torkkeli, M.; Mäkelä, T.; Serimaa, R.; ten Brinke, G.; Ikkala, O. *Science* **1998**, *280*, 557. (c) van Zoelen, W.; van Ekenstein, G. A.; Ikkala, O.; ten Brinke, G. *Macromolecules* **2006**, *39*, 6574. (d) Mäki-Ontto, R.; de Moel, K.; Polushkin, E.; van Ekenstein, G. A.; ten Brinke, G.; Ikkala, O. *Adv. Mater.* **2002**, *14*, 357.
(16) (a) Lefèvre, N.; Fustin, C. A.; Varshney, S. K.; Gohy, J. F. *Polymer* **2007**, *48*, 2306. (b) Hu, Z.; Jonas, A. M.; Varshney, S. K.; Gohy, J. F. *J. Am. Chem. Soc.* **2005**, *127*, 6526. (c) Lefevre, N.; Fustin, C. A.; Gohy, J. F. *Langmuir* **2007**, *23*, 4618. (d) Hu, Z.; Verheijen, W.; Hofkens, J.; Jonas, A. M.; Gohy, J. F. *Langmuir* **2007**, *23*, 116.
(17) (a) Peng, H.; Chen, D.; Jiang, M. *Langmuir* **2003**, *19*, 10989. (b) Gu, C.; Chen, D.; Jiang, M. *Macromolecules* **2004**, *37*, 1666. (c) Yao, X.; Chen, D.; Jiang, M. *Macromolecules* **2004**, *37*, 4211.
(18) Zhao, J. Q.; Pearce, E. M.; Kwei, T. K. *Macromolecules* **1997**, *30*, 7119.
(19) Kuo, S. W.; Chan, S.; Chang, F. C. *Macromolecules* **2003**, *36*, 6653.
(20) Kuo, S. W.; Huang, C. F.; Chang, F. C. *J. Polym. Sci., Part B: Polym. Phys.* **2001**, *39*, 1348.
(21) Zhang, S.; Painter, P. C.; Runt, J. *Macromolecules* **2004**, *37*, 2636.
(22) Berne, B. J.; Pecora, R. *Dynamic Light Scattering*; Plenum Press: New York, 1976.
(23) Meftahi, M. V.; Frechet, J. M. J. *Polymer* **1988**, *29*, 477.
(24) (a) Dai, J.; Goh, S. H.; Lee, S. Y.; Siow, K. S. *Polym. J.* **1994**, *26*, 905. (b) Zhou, X.; Goh, S. H.; Lee, S. Y.; Tan, K. L. *Appl. Surf. Sci.* **1997**, *119*, 60.
(25) Lee, J. Y.; Moskala, E. J.; Painter, P. C.; Coleman, M. M. *Appl. Spectrosc.* **1986**, *40*, 991.
(26) Zhao, J. Q.; Pearce, E. M.; Kwei, T. K. *Macromolecules* **1997**, *30*, 7119.
(27) Xiang, M.; Jiang, M.; Zhang, Y.; Wu, C.; Feng, L. *Macromolecules* **1997**, *30*, 2313.
(28) (a) Zhong, Z.; Guo, Q. *J. Polym. Sci., Part B: Polym. Phys.* **1999**, *37*, 2726. (b) Huang, J.; Li, X.; Guo, Q. *Eur. Polym. J.* **1997**, *33*, 659. (c) Zhong, Z.; Guo, Q. *J. Polym. Sci., Part A: Polym. Chem.* **1998**, *36*, 401.
(29) Purcell, K. F.; Drago, R. S. *J. Am. Chem. Soc.* **1968**, *89*, 2874.
(30) Guo, Q.; Harratsa, C.; Groeninckx, G.; Koch, M. H. J. *Polymer* **2001**, *42*, 4127.
(31) Guo, Q.; Harratsa, C.; Groeninckx, G.; Reynaers, H.; Koch, M. H. J. *Polymer* **2001**, *42*, 6031.
(32) Coleman, M. M.; Moskala, E. J. *Polymer* **1983**, *24*, 251.
(33) Moskala, E. J.; Varnell, D. F.; Coleman, M. M. *Polymer* **1985**, *26*, 228.
(34) Kuo, S. W.; Chang, F. C. *Macromol. Chem. Phys.* **2001**, *202*, 3112.
(35) Coleman, M. M.; Graf, J. F.; Painter, P. C. *Specific Interactions and the Miscibility of Polymer Blends*; Technomic Publishing: Lancaster, PA, 1991.
(36) Cesteros, L. C.; Meaurio, E.; Katime, I. *Macromolecules* **1993**, *26*, 2323.
(37) Kwei, T. J. *J. Polym. Sci., Polym. Lett. Ed.* **1984**, *22*, 307.
(38) (a) Yi, J. Z.; Goh, S. H. *Polymer* **2002**, *43*, 4515. (b) Luo, X. F.; Hu, X.; Zhao, X. Y.; Goh, S. H.; Li, X. D. *Polymer* **2003**, *44*, 5285.
(39) (a) Zheng, H.; Zheng, S.; Guo, Q. *J. Polym. Sci., Part A: Polym. Chem.* **1997**, *35*, 3161. (b) Zheng, H.; Zheng, S.; Guo, Q. *J. Polym. Sci., Part A: Polym. Chem.* **1997**, *35*, 3169. (c) Zhong, Z.; Guo, Q. *Polymer* **1998**, *39*, 517. (d) Guo, Q.; Zheng, H. *Polymer* **1999**, *40*, 637.
(40) Hamley, I. W. *Block Copolymers*; Oxford University Press: Oxford, 1999.
(41) Hasegawa, H.; Tanaka, H.; Yamasaki, K.; Hashimoto, T. *Macromolecules* **1987**, *20*, 1651.
(42) Guo, Q.; Liu, J.; Chen, L.; Wang, K. *Polymer* **2008**, *49*, 1737.

MA800703B